Static Behavior of Reinforced UHPFRC Beams with Minimal Cover Thickness

Author(s) & Affiliation:

Bartłomiej Sawicki* – Doctoral Assistant, Laboratory of Maintenance and Safety of Structures, École Polytechnique Fédérale de Lausanne (EPFL), Lausanne, Station 18, CH-1015, Switzerland, Email: bartek.sawicki@epfl.ch

Eugen Brühwiler – Professor, Laboratory of Maintenance and Safety of Structures, École Polytechnique Fédérale de Lausanne (EPFL), Lausanne, Station 18, CH-1015, Switzerland, Email: eugen.bruehwiler@epfl.ch

Abstract: Because of its high tensile strength and deformation capacity, UHPFRC (Ultra High Performance Fiber Reinforced Cementitious composite) can theoretically be used without any reinforcement bars or prestressing. However, for more economical design and for reasons of structural robustness, steel rebars should complement the UHPFRC leading to R-UHPFRC (Reinforced UHPFRC) structural elements. This paper focuses on the quasi-static behavior of UHPFRC beams reinforced with single steel rebar. The beams are full-scale elements (2 meters or 6.6 feet span, 0.4 meter of 1.3 feet height) inspired by a recently built R-UHPFRC railway bridge in Switzerland. They were prefabricated using one-way casting and external vibrations, to provide similar conditions as in mass production. The members are tested under quasi-static loading in four-point bending. Reinforcement cover thickness is only half of the bar diameter. Two bar diameters are tested (20mm/0.79in and 34mm/1.34in). The material properties variation within the member and the cover performance are discussed.

1. Introduction

The use of UHPFRC (Ultra High Performance Fiber Reinforced Cementitious composites) is rising around the world. The "art" of efficient design and construction of UHPFRC structures is to fully exploit the UHPFRC's mechanical properties. Thanks to the high amount of steel fibers in the UHPFRC, reinforcement bars are arranged only in the principal direction easing up the construction.

This paper focuses on the performance of Reinforced UHPFRC (R-UHPFRC) beams with minimal cover thickness of steel rebars. A UHPFRC short span railway underpass in Switzerland that was built in 2017 inspired the shape and sectional proportions of the specimens used in this research (Brühwiler, 2018). The cross-section of this structure is a 50mm (1.97in) thick slab with slightly haunched 500mm (19.68in) high ribs containing two rebars each.

The beams were tested under four point bending and the variation of material properties within the element was analyzed using a non-destructive magnetic testing method. The main goal of the experiments was to calibrate the loading levels for future fatigue tests on similar structural elements and to verify if the reinforcement cover thickness is sufficient.

2. Beams Casting and Material Testing

Two types of the beams have been casted, one type with one ribbed rebar ϕ20 (diameter 20mm or 0.79in) and the other with one ribbed rebar ϕ34 (diameter 34mm or 1.34in), see Figure 1. The beams were casted in horizontal position (as tested), pouring the fresh UHPFRC from the top at one end. Six external vibrators have been used to assure a good flow of the fresh UHPFRC mix. This way of casting is mocking up the real beam production. In addition, this way of casting produces more systematized fibre alignment over the length of the beam, contrary to casting with the bucket travelling along the whole length of the beam where the flow of the fresh material cannot be controlled. No balling of fibres was observed during fabrication of specimens.

The six beams were casted independently. Commercially available UHPFRC mix Holcim710© was used, with 3.8% by volume of 13mm (0.51in) straight steel fibres with aspect ratio 65. The minimum age at the moment of testing was three months. The cement hydration in UHPFRC is advanced after 28 days and stops almost completely after 90 days (Habel, Viviani, Denarié, & Brühwiler, 2006). Thus, the age has no influence on material properties. To confirm, the material from the two castings was tested in four point bending according to the Swiss standard for UHPFRC (SIA 2052, 2016) at the age of 28 and 90 days (leading to four testing series), six plates in each series. Following properties were searched: (1) elastic tensile limit stress f_{Ute}, (2) tensile strength f_{Utu}, (3) hardening strain ε_U and (4) modulus of elasticity E_{Ut}. The results presented in Table 1 showing that after 28 days no strength increase can be noticed. The average compressive resistance was f_{Uc} = 148.68 MPa (3105kips/ft²).

Both types of steel reinforcement bars used in this experimental series were B500B with the following properties: (1) characteristic yielding strength f_{sk} = 500MPa (10442kips/ft²), (2) ratio of characteristic yielding strength to tensile strength f_{tk} / f_{sk} ≥1.08 and (3) strain at tensile strength ε_{uk} ≥ 5%. No material testing has been done for the reinforcement.

Table 1 Test Results (average values of 2 tests) of UHPFRC After 28 and 90 Days

	f_{Ute} [MPa]([kips/ft²])	f_{Utu} [MPa]([kips/ft²])	ε_U [‰]	E_{Ut} [GPa]([kips/in²])
28 days	6.35 (133)	11.75 (245)	3.66	41.96 (6085)
90 days	6.20 (129)	12.30 (257)	3.41	41.89 (6076)
Average	6.28 (131)	12.02 (251)	3.53	41.92 (6080)

3. Quasi-static Testing

The beams were subjected to actuator displacement-controlled four-point bending, as presented in Figure 1. During the test, the beams were unloaded multiple times to determine the beam stiffness. Different spacing of force application points was used to obtain appropriate shear-bending moment balance.

Beam S1 failed in shear. To avoid shear failure, the predominant shear zone of Beams S2 and S3 was strengthened by a steel tape. For Beams S4 and S5, the distance between force application points was reduced (Figure 1) to increase the bending moment under the same shear force. It was further reduced for Beam S6A where the bending moment-shear balance was close and yielding of reinforcement occurred before shear failure prevailed.
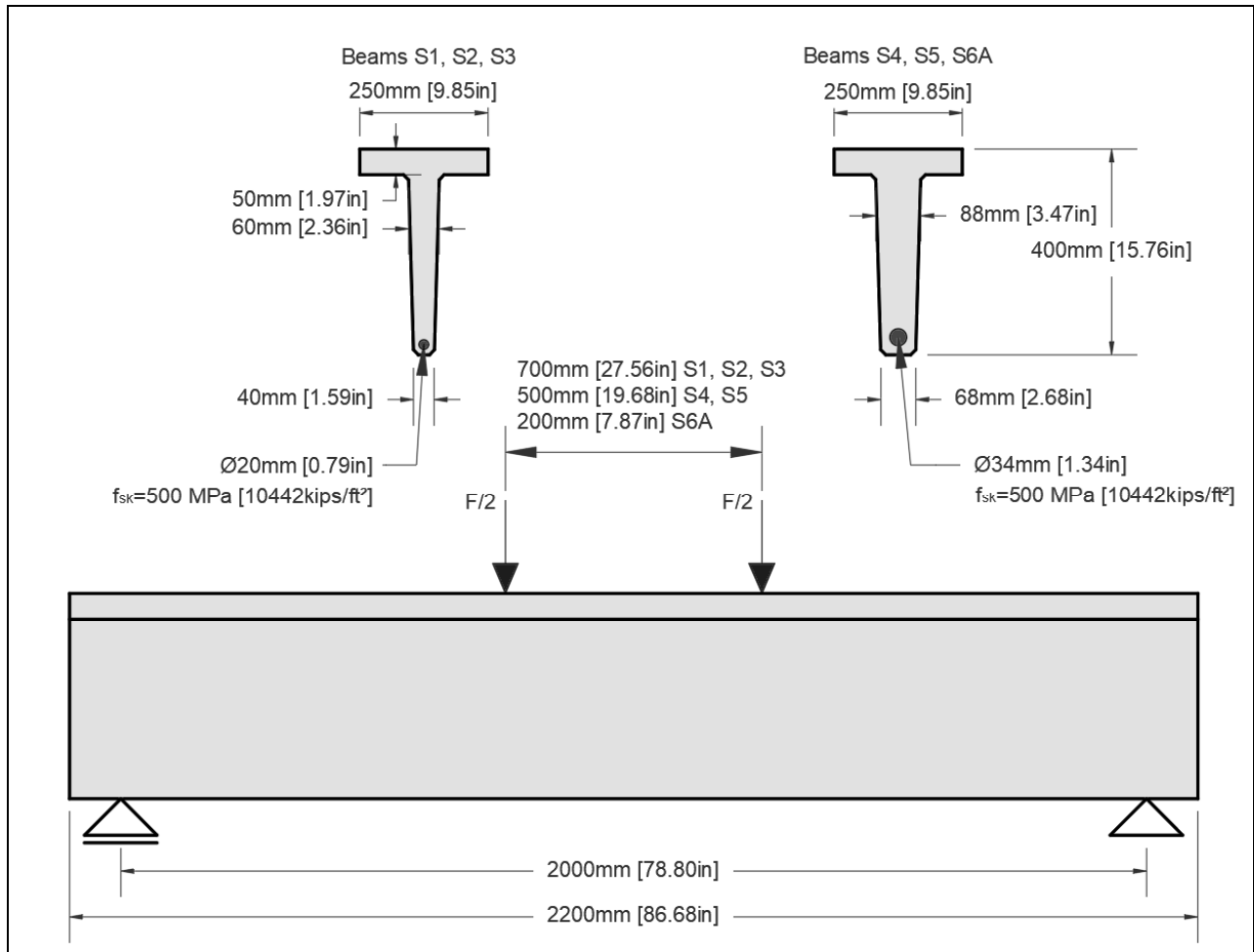
Figure 1. Test Scheme

Both Beams S2 and S3 failed in bending. Since in case of Beam S2 the critical crack passed through one of the extensometers, this beam shall be discussed in detail. The scheme of extensometers and crack location are shown in Figure 2 and the results in Figure 3.

The bottom of Figure 3 presents the force - deflection curve. The deflection is obtained from the measured displacement at mid-span less the measured average displacement of the supports. The first portion of the curve presents the elastic domain (up to ca. 90kN or 20.2kips) with constant slope when the UHPFRC in the whole cross-section behaves linear elastically. Then, gradual decrease of the slope is observed corresponding to beam stiffness decrease due to UHPFRC hardening in the tensile zone. Unloadings allow to identify residual deflection. This non-linear behavior continues until the maximum resistance is reached (335kN or 75.3kips), and beyond, resistance gradually decreases with increasing deflection. At this stage, localized discontinuity, i.e. fictitious crack with stress transfer by the fibers, is visible in the UHPFRC. Noteworthy, this discontinuity cannot be called 'crack' as stress transfer still exists between crack faces.

The R-UHPFRC beams present significant post-peak ductility. To avoid damage of LVDTs and extensometers, they were removed after peak was reached. Loading was continued, and the deflection was calculated on the basis of the measured actuator displacement using cubic extrapolation of the deflection measured by LVDTs during the first part of the test. The observed

post-peak resistance plateau at the level of about 280kN (63.0 kips) or 80% of the maximum resistance is due to fictitious crack growth and rebar yielding.

In the upper part of Figure 3, apparent strains measured by extensometers are shown. The extensometer base was 100mm (3.93in). The differences in read-outs are exclusively due to material non-uniformity. In the first portion of graph, all the curves are parallel indicating similar stiffness. The point where the curve is no longer linear indicates the limit of elasticity of UHPFRC. For the extensometers 2 and 6 the elasticity limit is difficult to identify and the decrease of stiffness is present from the first load steps. They also show lower post-elastic (strain-hardening) stiffness. This might indicate local zones of lower resistance, most likely due to the fibre alignment. The other extensometers indicate the elasticity limit at a force value ranging from 30 to 110 kN (6.7 to 24.7kips) with similar stiffness. Those curves show similar strain-hardening stiffness as well. Detailed analysis of material variation within the beam is discussed in Section 4.
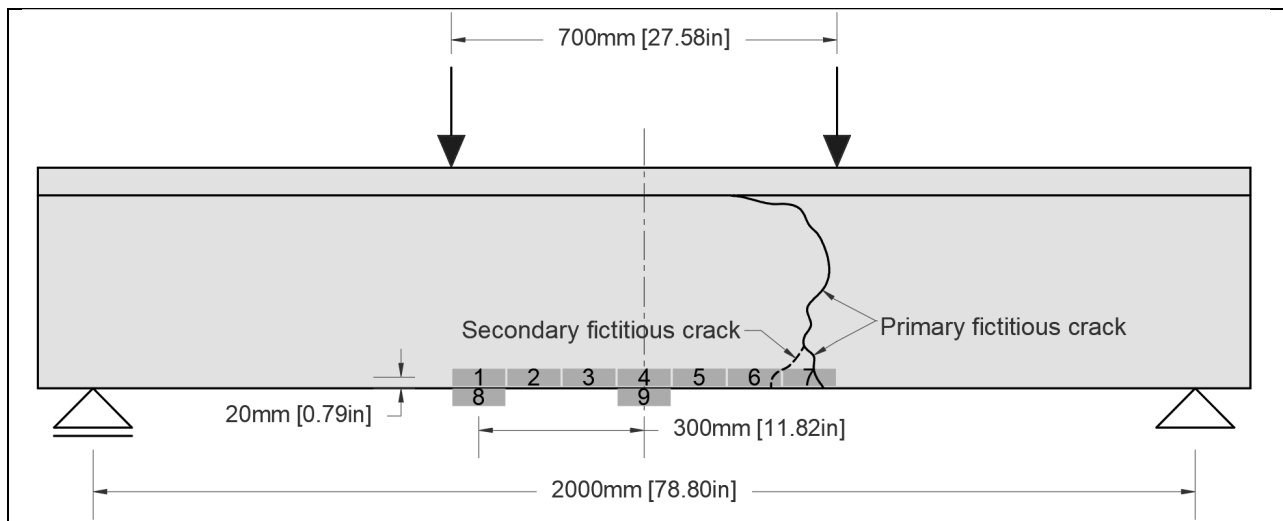

Figure 2. Deployment of Extensometers and Crack Pattern of Beam S2

The critical fictitious crack appeared in the cross section where extensometer 7 was installed (rightmost extensometer). This is quite unexpected as no loss of stiffness could been noticed prior to that. When the discontinuity was localised, loss of global resistance followed. The apparent increase of strain for this extensometer is due to the opening of the fictitious crack (it should be noted that the beam deflection was still rising due to actuator displacement). Unloading of the other sections is visible. Interestingly, at force level of about 310kN (69.7kips) the main discontinuity stops to open and secondary branch is created (extensometer 6). This might be due to the non-uniformity of UHPFRC along the beam height. The propagating discontinuity might have reached a stronger zone, thus the weak front opens nearby. After this point, the beam was unloaded completely. The discontinuity near extensometer 6 closed partially, while the opening of crack registered by extensometer 7 remains the same. The post-peak part of the force – deflection curve was not registered as the extensometers were dismantled before to avoid their damage.

4. Material Variation Within the Beam

It is well known that the properties of UHPFRC depend on fibre content and orientation, see e.g.: (Doyon-Barbant & Charron, 2018; Oesterlee, 2010; Wuest, 2007) which in turn depend on the

element's geometry, way of casting or material workability. For Beam S3, detailed investigation of magnetic conductivity with a coil was conducted to study the fibre orientation. Steel fibres are induced with the magnetic field. Thus, the higher the fibre content and the more they are aligned, the higher is the measured magnetic inductance (Pimentel & Nunes, 2016). This testing method should be considered as a qualitative information rather than quantitative, unless calibration with destructive testing is done.
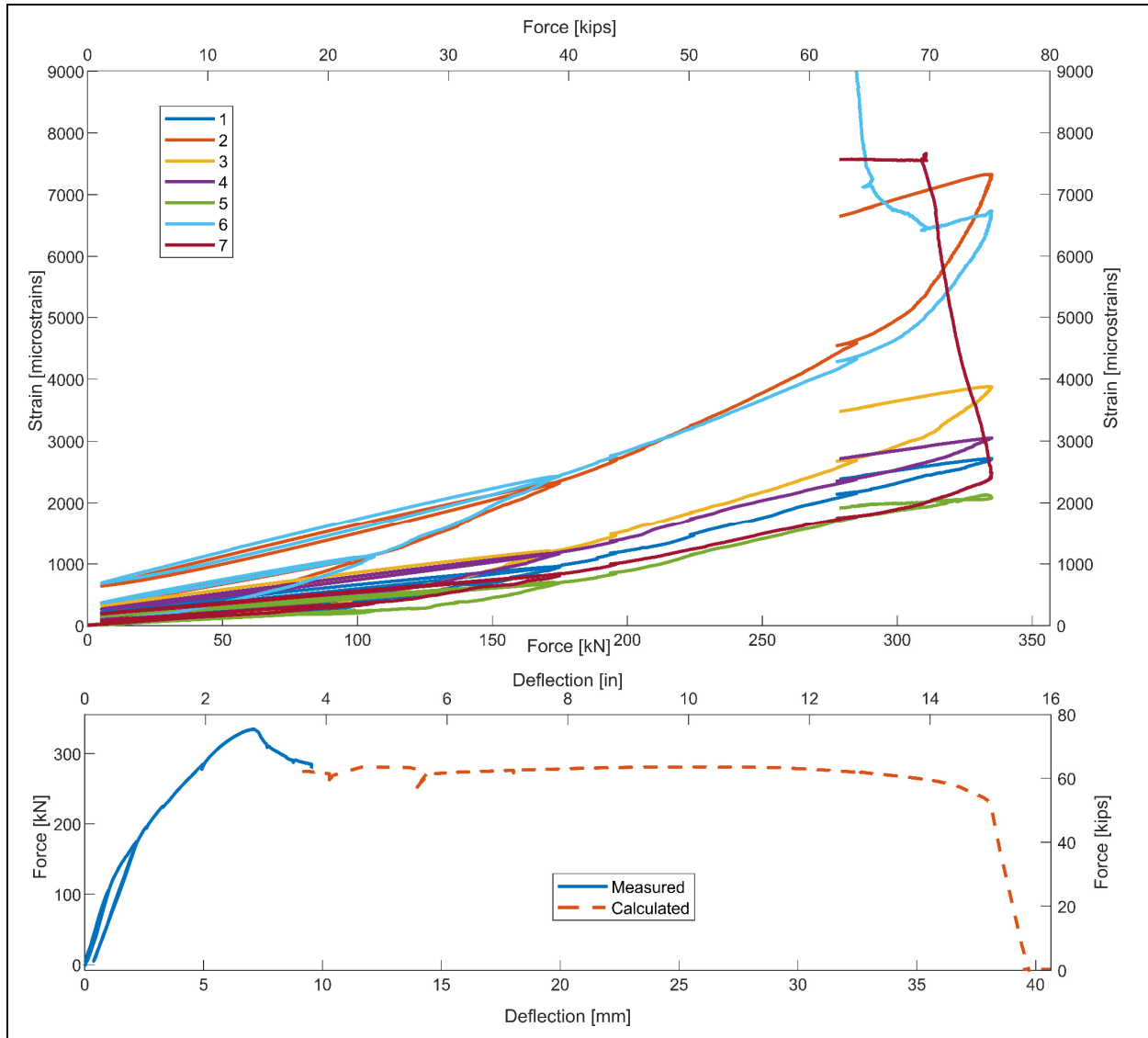
Figure 3. Force-deflection and Force-strain Curves, Test S2

The fibre content and orientation of UHPFRC could not been measured objectively in the vicinity of the reinforcement bar which produces a large magnetic inductance, thus falsifying the results. Since the extensometers were installed at the level of the reinforcement bar (20mm or 0.79in from the bottom), the closest measurement point value is used as most reliable value. In this test, the critical crack occurred outside the extensometer 6, thus just at the border of the constant bending moment region (see Figure 4).
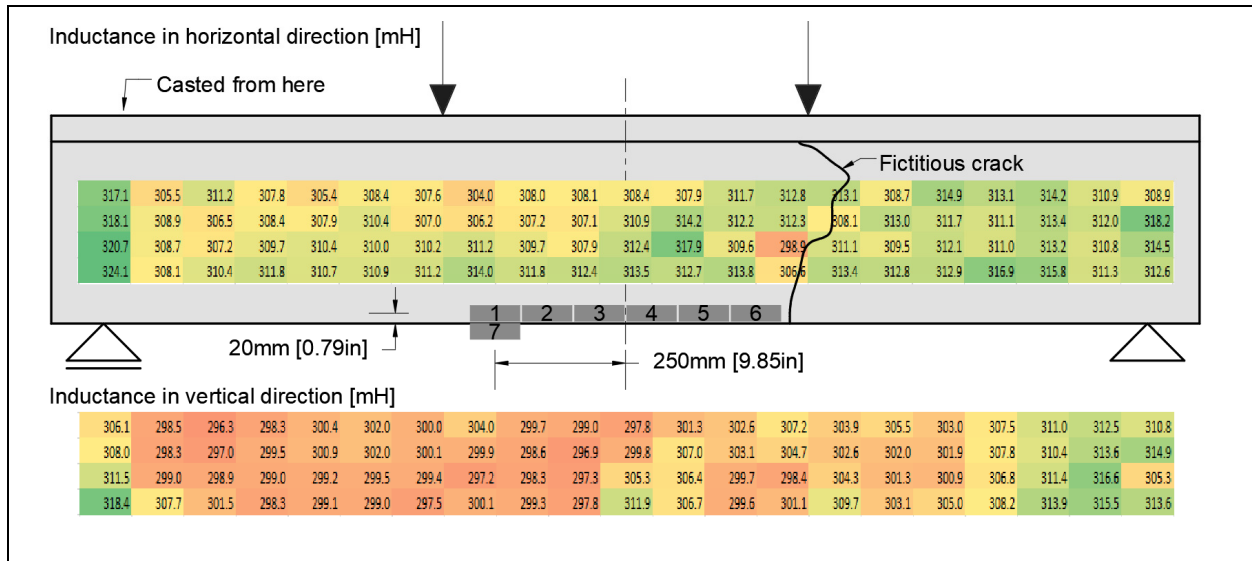
Figure 4. Inductance Measurements on Beam S3

Table 2. Apparent Secant Moduli and Inductance Variation, Beam S3

	Force [kN]([kips])	29 (6.5)	85 (19.1)	170 (38.2)	246 (55.3)	288 (64.7)	342 (76.9) (Peak)	Inductance [mH]
Sensor	Theoretical stress [MPa] [kips/ft²]	4.5 93	8.3 173	9.9 208	11.7 244	12.6 263	-	
1	Strain [microstrains]	133	427	1232	2374	3062	4009	311.8
	Apparent Modulus [GPa] [kips/in²]	33.6 4873	19.5 2828	8.1 1175	4.9 711	4.1 595	- -	
2	Strain [microstrains]	109	392	1151	2073	2521	2940	312.4
	Apparent Modulus [GPa] [kips/in²]	41.2 5975	21.2 3075	8.6 1247	5.6 812	5.0 725	- -	
3	Strain [microstrains]	83	265	1143	2045	2610	4344	313.5
	Apparent Modulus [GPa] [kips/in²]	53.8 7803	31.4 4554	8.7 1262	5.7 827	4.8 696	- -	
4	Strain [microstrains]	112	413	1233	2171	2668	6063	312.7
	Apparent Modulus [GPa] [kips/in²]	39.9 5787	20.1 2915	8.1 1175	5.4 783	4.7 682	- -	
5	Strain [microstrains]	99	282	887	1508	1917	2433	313.8
	Apparent Modulus [GPa] [kips/in²]	45.2 6556	29.5 4279	11.2 1624	7.7 1117	6.6 957	- -	
6	Strain [microstrains]	145	587	1599	2917	3608	4685	306.6
	Apparent Modulus [GPa] [kips/in²]	30.9 4482	14.2 2059	6.2 899	4.0 580	3.5 508	-	

Figure 4 shows high fiber content next to the location where the fresh UHPFRC was filled in the formwork. Then, with the flow of fresh mix, the fibers are oriented more uniformly, with the preference of horizontal direction along the flow direction of the fresh mix. The vertical direction orientation is much weaker, indicating lower tensile resistance. Towards the end of beam, the fiber content becomes higher and more uniform regarding horizontal and vertical directions, up to the end of the beam where the accumulation of fibers can be noticed. This comes from the use of a fluid mix (average slump-flow 625mm or 24.60in) and imposed vibrations, to improve the workability and casting of UHPFRC.

The fictitious crack is first apparent where the fiber content is lowest. Then, it deviates to the right, outside of the constant bending moment zone looking for the weakest trajectory. Beyond, it shifts towards the left, being either attracted by the force or the fiber orientation. In the vicinity of an appearing first fictitious crack, localized extensive strains in the reinforcement bars are produced (Oesterlee, 2010), which will eventually lead to rebar fracture. Thus, the fiber content and orientation actually determine the location of beam failure.

In Table 2, the magnetic inductance, strains at given force levels as well as calculated stresses and apparent secant moduli are given for each senor. The stress values are calculated using recorded force and assuming material properties from material tests. The secant modulus was determined as the slope of line between the origin of coordinate system and the measured strain for the calculated stress.

The table reveals that there exists a relationship between the inductance measurements and the secant modulus, however the correlation is not strong. The inductance measured above extensometer 6 is the lowest, and so is the apparent modulus. The values measured using NDT and extensometers are similar for sensors 2 and 4. However, although the measured inductance above extensometers 3 and 5 are similar, the initial modulus is higher for extensometer 3 and the strain-hardening secant is higher for extensometer 5. These discrepancies might come from the fact that the NDT measurements were not taken exactly at the level of the extensometer, as well as that there was only one measurement point per extensometer which might not be enough to capture properly local material variations.

Table 3. Cover Strains at Peaks for 6 Tests

Test	Rebar	Moment [kNm]/[kips·ft] (failure mode)	Mid-span strain [microstrain]			Section 1 (30 cm from the middle) strain [microstrain]		
			Rebar level	Cover	Difference [%]	Rebar level	Cover	Difference [%]
S1	*φ20*	109.8/81.0 (shear)	3390	3613	6	4431	3793	-17
S2	*φ20*	108.7/80.2 (bending)	3051	3838	26	2717	5027	85
S3	*φ20*	109.2/80.5 (bending)	4344	-	-	4009	3898	-3
S4	*φ34*	195.5/144.2 (shear)	2091	2821	35	1960	2993	53
S5	*φ34*	179.5/132.4 (shear)	2590	2541	-2	2776	3291	19
S6A	*φ34*	230.4/169.9 (shear)	2186	4138	89	3632	5630	55

5. Cover Performance

As presented in Figure 2 and Figure 4, the extensometers were installed externally on the UHPFRC surface at the level of rebar axis. Lower strains measured on the UHPFRC cover with respect to measured rebar strains would indicate that the bond is not perfect, however due to inherent non-

uniformity of UHPFRC this difference needs to be assessed carefully This reasoning is valid only with the perfect bond on the rebar level, which can be assumed with UHPFRC (Oesterlee, 2010). In Table 3, the strain profiles at peak loads are presented.

The results show variation that might be due to differences in UHPFRC stiffness as discussed previously. Additionally, the presence of the rebar in the UHPFRC bulk material obviously influences the flow and thus the orientation of fibres in the vicinity of the rebar (Oesterlee, 2010). However, no cover spalling or horizontal microcracking were noticed, thus it may be stated that the cover of $\phi/2$ does not influence the resistance of beams tested.

6. Conclusions

This paper presented the flexural behavior of UHPFRC beams with a single reinforcement bar. It was demonstrated that (1) the thickness of reinforcement cover equal to half of bar diameter is sufficient from a mechanical viewpoint, and (2) inherent local variation of mechanical properties of UHPFRC is confirmed. These variations however do not decrease the overall performance of the structural element, but indicate the zone where failure occurs.

7. References

Brühwiler, E. (2018). "STRUCTURAL UHPFRC" TO ENHANCE BRIDGES. *Proceedings of the 2nd International Conference on UHPC Materials and Structures UHPC 2018 - China*, *129*, 140–158.

Doyon-Barbant, J., & Charron, J.-P. (2018). Impact of fibre orientation on tensile, bending and shear behaviors of a steel fibre reinforced concrete. *Materials and Structures*, *51*(6), 157.

Habel, K., Viviani, M., Denarié, E., & Brühwiler, E. (2006). Development of the mechanical properties of an Ultra-High Performance Fiber Reinforced Concrete (UHPFRC). *Cement and Concrete Research*, *36*(7), 1362–1370.

Oesterlee, C. (2010). *Structural Response of Reinforced UHPFRC and RC Composite Members*. École polytechnique fédérale de Lausanne, Lausanne, Switzerland.

Pimentel, M., & Nunes, S. (2016). Determination of the fibre content and orientation in UHPFRC layers using NDT – application to the simulation of the behaviour of strengthened beams (p. 7). Presented at the 8th International Conference on Bridge Maintenance, Safety and Management (IABMAS), Foz do Iguacu, BRAZIL.

SIA 2052. (2016, March). SIA 2052 / 2016 F - Béton fibré ultra-performant (BFUP) - Matériaux, dimensionnement et exécution.

Wuest, J. (2007). *Comportement structural des bétons de fibres ultra performants en traction dans des éléments composés*, École polytechnique fédérale de Lausanne, Lausanne, Switzerland.

8. Acknowledgment